

# Nephrocystin-4 is required for pronephric duct-dependent cloaca formation in zebrafish

Krasimir Slanchev<sup>1</sup>, Michael Pütz<sup>1,†</sup>, Annette Schmitt<sup>1</sup>, Albrecht Kramer-Zucker<sup>1</sup>  
and Gerd Walz<sup>1,2,\*</sup>

<sup>1</sup>Renal Division, University Freiburg Medical Center, Freiburg, Germany and <sup>2</sup>Center for Biological Signaling Studies (bioss), Freiburg, Germany

Received April 4, 2011; Revised and Accepted May 10, 2011

***NPHP4* mutations cause nephronophthisis, an autosomal recessive cystic kidney disease associated with renal fibrosis and kidney failure. The *NPHP4* gene product nephrocystin-4 interacts with other nephrocystins, cytoskeletal and ciliary proteins; however, the molecular and cellular functions of nephrocystin-4 have remained elusive. Here we demonstrate that nephrocystin-4 is required for normal cloaca formation during zebrafish embryogenesis. Time-lapse imaging of the developing zebrafish pronephros revealed that tubular epithelial cells at the distal pronephros actively migrate between the yolk sac extension and the blood island towards the ventral fin fold to join the proctodeum and to form the cloaca. *Nphp4*-deficient pronephric duct cells failed to connect with their ectodermal counterparts, and instead formed a vesicle at the obstructed end of the pronephric duct. Nephrocystin-4 interacts with nephrocystin-1 and Par6. Depletion of zebrafish *NPHP1* (*nphp1*) increased the incidence of cyst formation and randomization of the normal body axis, but did not augment cloaca malformation in *nphp4*-deficient zebrafish embryos. However, simultaneous depletion of zebrafish Par6 (*pard6*) aggravated cloaca formation defects in *nphp4*-depleted embryos, suggesting that *nphp4* orchestrates directed cell migration and cloaca formation through interaction with the Par protein complex.**

## INTRODUCTION

Nephronophthisis (NPHP), an autosomal recessive cystic kidney disease often presenting with polydipsia, polyuria, anemia and growth retardation, is one of the most frequent genetic causes of end-stage kidney failure in children and young adults. The most prominent histological alterations are abnormalities of the tubules with thickening of the basement membrane and interstitial fibrosis, progressing to cysts positioned at the corticomedullary junction in more advanced stages (1). Contrary to polycystic kidney disease, NPHP typically is associated with normal or diminished kidney size. Mutations in more than 10 genes (*NPHP1–11*, *NPHPL1*) have been identified as the cause of NPHP (1–4). In zebrafish, loss of NPHP genes function causes a stereotypical set of developmental changes, including an abnormal body curvature, heart edema, defects in cilia length or function and pronephric cyst formation (5–8). Primary cilia are sensory

organelles that connect mechanosensory, visual, osmotic and other stimuli to signaling cascades controlling cell cycle, epithelial cell polarity and organ development (9). On the basis of their presence in the cilium and/or the basal body, the abnormalities caused by NPHP genes in vertebrates are attributed to defects in ciliary function.

*NPHP4* mutations cause familial juvenile NPHP type 4. It accounts for about 2% of NPHP cases and can result in isolated cystic kidney disease or cystic kidney disease with oculomotor apraxia (Cogan syndrome), retinitis pigmentosa (Senior–Loken Syndrome, SLS) and liver fibrosis. The *NPHP4* gene product nephrocystin-4 interacts with multiple adaptor and signaling components, but also with the gene products of *NPHP1* (nephrocystin-1), *NPHP8* (RPGRIP1L) and components of the Par polarity complex (10). Nephrocystin-4 localizes to cell–cell junctions, basal body and transition zone of primary cilia as well as to the cortical actin cytoskeleton of epithelial cells, implying variable functions at these different sites (6,10–13).

\*To whom correspondence should be addressed at: Medizinische Klinik IV, Hugstetter Str. 55, 79106 Freiburg, Germany. Tel: +49 76127032500; Fax: +49 76127032450; Email: gerd.walz@uniklinik-freiburg.de

<sup>†</sup>Present address: Clinical Neuroimmunology Group, Department of Neurology, Philipps-University, Marburg, Germany.

The functional kidney of the zebrafish larva, the pronephros, consists of a capillary tuft connected to two ducts, which run bilaterally along the body axis and fuse at the cloaca opening. The two pronephric ducts consist of highly polarized epithelial cells, carrying one or more motile cilia on the apical membrane. These directionally beating cilia generate a fluid-flow that contributes to lumen patency and urine excretion through the cloaca. Interference with urine flow by disruption of ciliary function or mechanical obstruction of the pronephric duct causes pronephric cyst formation (14–16). The cloaca in fish is the common opening of the urinary and the gastrointestinal tracts to the environment. In zebrafish, the cloaca forms around 24 h post-fertilization (hpf), when epidermal cells fuse with the distal pronephric duct. Markers such as *prdm1*, *vox1*, *evx1*, *tbx2b* and *gata3* label the contributing epidermal and pronephric components during this stage (17,18). Shaping of the cloaca requires extensive epithelial remodeling and orchestrated apoptosis of epidermal cells, which enables the duct to open to the environment. Bone morphogenetic proteins (Bmp) provide the main cell-patterning cues for the cloaca-forming events, and alterations in Bmp levels lead to defective cloaca formation (17,18).

Here, we describe the role of nephrocystin-4 in zebrafish pronephros development and function. We demonstrate that the morpholino oligonucleotide (MO)-mediated knockdown of zebrafish *nphp4* affects cilia formation and function, leading to disturbed left–right asymmetry and pronephric cyst formation. Our analysis revealed an unexpected role of *nphp4* in cloaca formation, implying a cross-talk between Bmp and *nphp4* signaling. *In situ* hybridization (ISH) with marker genes expressed in the cloaca region demonstrated that *nphp4* depletion did not affect the specification of the ectodermal and pronephric components of the future cloaca. *In vivo* investigation of the cloaca development revealed that the directed migration of distal pronephric cells towards the site of fusion with ectodermal cells was abrogated in *nphp4*-deficient zebrafish embryos, preventing programmed cell death of ectodermal cells. This defect was aggravated by simultaneous depletion of the polarity protein Par6, suggesting that *nphp4* orchestrate directed cell migration and cloaca formation through interaction with the Par protein complex.

**RESULTS**

**Identification and cloning of *nphp4***

To identify full-length zebrafish *nphp4* homolog, we used BLAST searches of the human *NPHP4*, comparing protein sequence against zebrafish Ensemble8 Genome sequences at the Sanger Institute. The best hit was located on chromosome 8, covering two partially overlapping predicted gene sequences, ENSDART00000100063 and ENSDART00000111181. Combining these two sequences, we obtained full-length zebrafish *nphp4*, which consists of 1357 amino acids and is 43.8% identical to its human ortholog (Fig. 1A). As its human counterpart, zebrafish *nphp4* does not contain known conserved protein domains. Interestingly, amplification of the sequence from mRNA isolated from embryos 2 days after fertilization yielded three different PCR products,

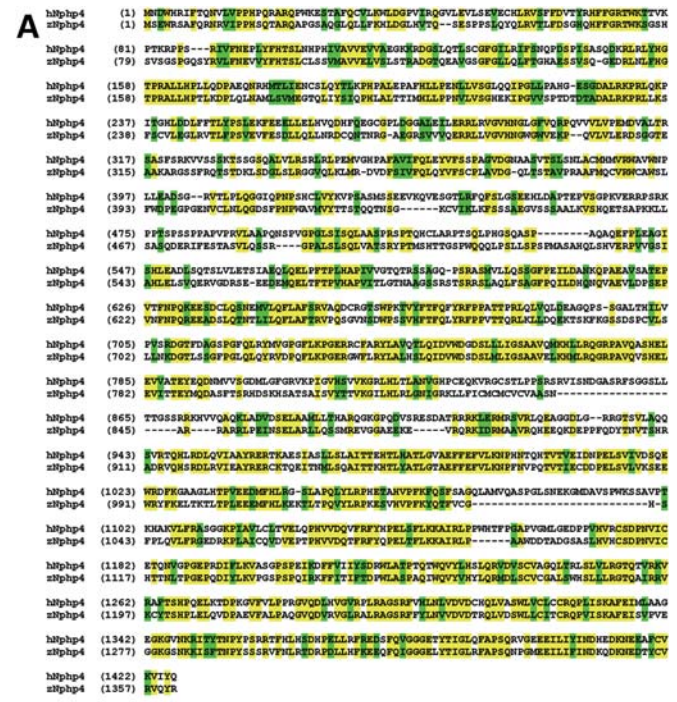


**Figure 1.** Cloning and expression pattern of zebrafish *nphp4* homologue. (A) The zebrafish nephrocystin-4 consists of 1357 amino acids, and is 43.8% identical to its human homolog. (B–D) *In situ* hybridization with an *nphp4* probe shows that it is ubiquitously expressed during the studied stages. At the 6-somite stage, *nphp4* mRNA is enriched in the zebrafish laterality organ, Kupfer's vesicle (arrowhead in B), and in the distal end of the pronephric duct at 24 h post fertilization (arrow in C).

which were identified as alternative splice variants of *nphp4*. The longest one, referred here as splice variant 1, contained exons 1–31 of the predicted sequence, giving rise to a full-length protein. In the second one (splice variant 2), exon 6 was directly spliced to the middle of the exon 22, excluding exons 7–21. This shorter transcript contained a premature STOP codon, giving rise to a 390 amino acid-long protein. Based on the strength of the PCR bands, variants 1 and 2 were present at similar levels, but more abundant than variant 3 (data not shown).

**Expression pattern of Zebrafish *nphp4***

To determine the expression pattern of zebrafish *nphp4*, we generated an antisense RNA probe and performed ISH.

Zebrafish *nphp4* was expressed ubiquitously at low levels during the first 2 days of development with elevated expression levels in the Kupffer's vesicle (KV) at the 6-somite stage (Fig. 1B–D, arrowhead) and the distal part of the pronephros at 24 h post-fertilization (hpf) (Fig. 1C, arrows).

### Phenotypic changes after knockdown of Zebrafish *nphp4*

To study the function of *nphp4* during zebrafish embryonic development, we designed antisense MO, targeting the translation initiation site of *nphp4* mRNA (*nphp4* ATG) and a splice MO targeting the splice donor site of exon1. Both MOs gave similar phenotypes; however, experiments with the translation blocking MO were more consistent, and subsequently used unless noted otherwise. To demonstrate the efficiency of the translational block, we injected mRNA, containing a fragment of zebrafish *nphp4* with the MO binding region fused to green fluorescent protein (GFP) in combination with the *nphp4* ATG MO. Subsequent fluorescent imaging of the injected embryos demonstrated that the MO efficiently prevented GFP translation (Fig. 2G, H). Injections of this MO into fertilized eggs produced embryonic defects resembling those observed after knockdown of other polycystic kidney disease (PKD) genes in zebrafish (8,16), including abnormal body curvature, hydrocephalus, pericardial edema and pronephric cysts (Fig. 2A–D). Using transgenic fish lines expressing GFP in the glomerulus (*wt1b:gfp*) (19) (Fig. 2D) and the pronephric duct (*cldn2b:lyn-gfp*) (20) (Fig. 2E, F, arrowheads), we detected cyst formation in the glomerular region (arrowheads in Fig. 2B–D) as well as a dilated pronephric duct (Fig. 2E and F, arrowheads). In addition, formation of a vesicle at the distal end of the pronephric duct was noted (arrows in Fig. 2B and F, quantified in Fig. 2I). While body curvature was observed in all embryos in an MO dose-dependent fashion, the number of embryos developing pronephric cysts strongly varied (between 25 and 80%), depending on the fish strain (e.g. the zebrafish TL strain developed more cysts than the zebrafish strain AB/TL). Over-expression of full-length human or zebrafish *nphp4* caused concentration-dependent embryonic defects and failed to rescue the cloaca defects of *nphp4* morphants, indicating that a precise balance between different *nphp4* isoforms might be required to rescue the MO-mediated defects.

### Morphant cilia phenotype

Defects in genes important for cilia development, e.g. intraflagellar transport (IFT) proteins, often lead to pronephric cyst formation in zebrafish (16,21). To examine the effect of *nphp4* knockdown on ciliogenesis, we stained the KV and the pronephric duct of morphant and wild-type (WT) embryos for acetylated tubulin. Cilia of morphant zebrafish were significantly shorter than the cilia of their WT siblings (Fig. 3A–F) (Student's *t*-test,  $P < 0.001$ ). While the average number of cilia in the KV of morphant embryos was almost two times lower than that of the cilia in the WT embryos (21.6 in morphant versus 38.3 in wild-type embryos), there was no significant difference in cilia numbers on the cells of the pronephric duct. Nevertheless, the size of the KV of the

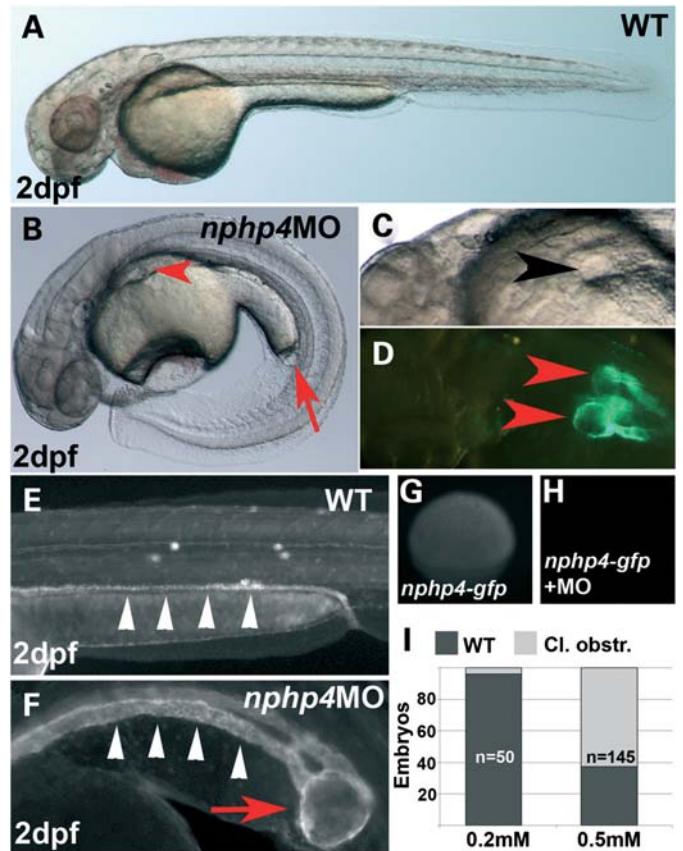


**Figure 2.** Depletion of *nphp4* causes body curvature, cyst formation and cloaca obstruction in zebrafish embryos. (A–D) Embryos injected with morpholino oligonucleotides (MO) targeting *nphp4* develop an abnormal body curvature (B), heart edema (B), pronephric cysts (arrowhead in B–D) and a vesicle obstructing the cloaca (arrow in B) at 2 days post-fertilization. (C and D) Magnification of the dorsal trunk region of the MO-injected embryos; pronephric cysts (arrowheads), formed laterally from the glomerulus, visible under DIC and fluorescent microscopy, using the *wt1b:gfp* transgenic line. (E and F) Fluorescent images of wild-type and *nphp4* MO-injected embryos of the *Cldn2b:lyn-gfp* transgenic line. The pronephric duct in MO-injected embryos is obstructed (arrow in F), promoting dilation (arrowheads in F) and cyst formation. (G and H) The *nphp4* AUG MO inhibits translation of *nphp4* mRNA *in vivo*. Embryos injected with a fusion mRNA composed of the N-terminal part of *nphp4* and GFP, express fluorescent fusion protein (G). The translation of the fusion mRNA is blocked when the construct is co-injected with the *nphp4* AUG MO (H). (I) Embryos injected with *nphp4* MO develop cloaca defects in a concentration-dependent manner.

morphants was slightly smaller (Supplementary Material, Fig. S2); therefore, a more general developmental defect could account for the observed ciliary differences. Two days after fertilization, the cilia in the dilated pronephric ducts of *nphp4* MO-injected embryos were disoriented and often appeared curly (data not shown). Consistent with an abnormal body axis associated with defective KV fluid flow (22), heart looping was randomized in the *nphp4* morphants (Fig. 3G–I, K). These findings suggest that zebrafish *nphp4* plays a role in cilia formation and/or function.

### Defective cloaca formation in *nphp4*-deficient Zebrafish

Investigating the defects of *nphp4* MO-injected embryos, we noticed the presence of a vesicle at the distal end of the

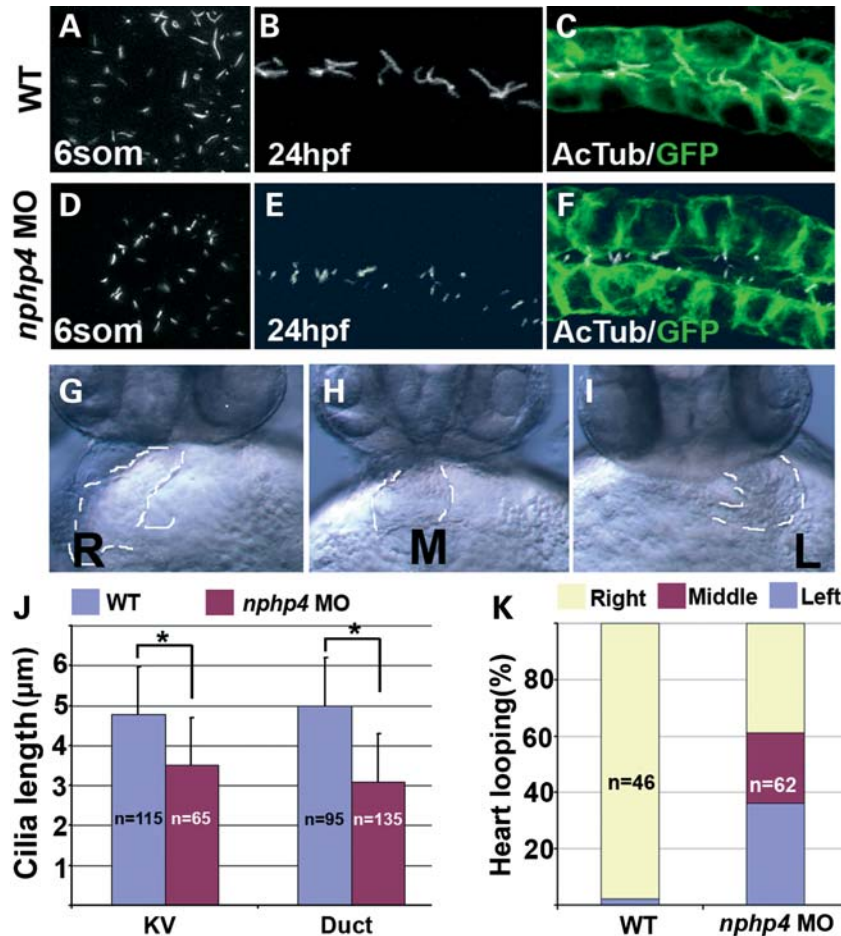


**Figure 3.** Injections of *np4* morpholino in zebrafish embryos cause defects in cilia formation and function. (A and D) Images of acetylated tubulin-stained cilia in the Kupffer's vesicle (KV) of 6-somite-stage zebrafish embryos. Each image is a projection of a confocal Z-stack. The cilia of MO-injected embryos (D) appear less in number and shortened compared with control embryos (A). Cilia length of three different embryos from each sample was quantified in (J). (G–I) Images of 2-day-post-fertilization zebrafish embryos with their hearts looped to the right (G), to the left (H) or without heart looping (I). The heart tube is outlined with dashed lines. The orientation of the heart looping was quantified in (K). While the hearts of almost all wild-type embryos looped to the right, MO-injected embryos failed to break the body symmetry, and showed no bias in the heart orientation. (B, C, E and F) Images of acetylated tubulin-stained cilia in GFP-labeled pronephric duct of wild-type and *np4* MO-injected, 1-day-old embryos. Cilia of the morphants (E, F) appear shorter in comparison to their non-injected siblings (B and C), quantified in (J).

pronephric duct indicative of cloaca malformation (Fig. 2). Since mechanical obstruction of the pronephric ducts close to the cloaca causes cyst formation in the proximal pronephros (23), we hypothesized that a failure to generate patent distal pronephric ducts contributed to proximal cyst formation in *np4*-deficient zebrafish embryos. To determine whether cloaca malformation was the result of incorrectly specified tissue, we performed ISHs for *gata3*, *tbx2b*, *prdm1*, *vox1* and *evx1* (Fig. 4). The probes for *gata3* and *tbx2b* mark the distal pronephros (17). The expression of *prdm1* and *vox1* in ectodermal cells of the fin ridges and the cloaca requires intact Bmp signaling (18,24), while *evx1* is expressed in the distal pronephros as well as ectodermal cells (25). Although distorted by cloaca defects and obstruction of the terminal pronephros, expression of *evx1*, *gata3* and *tbx2b* appeared largely intact (Fig. 4). The *np4* MO-injected zebrafish embryos displayed two *prdm1* positive domains. One domain marked the ectoderm, the other region localized to the distal pronephros partially displaced by the vesicle at the distal end of the

pronephros (Fig. 4A and B). These findings suggest that both the distal pronephric duct and the ectodermal tissue forming the cloaca (proctodeum) were correctly specified even in the absence of *np4* (Fig. 4A–L). When the ISHs were repeated for *oval*, an IFT88-deficient zebrafish mutant with defective ciliogenesis, the distribution of the markers, including their position in respect to the ectoderm did not significantly deviate from wild-type embryos (Fig. 4C, F, I, L). Since *oval* mutants did not display cloaca malformations despite an abnormal body curvature and severe cysts formation, these results indicate that the cloaca defects observed in *np4* MO-injected embryos occur independently of cell fate specification and ciliogenesis.

Defective Bmp signaling causes abnormal cloaca development (18). However, these studies did not investigate the relationship between cloaca formation and zebrafish pronephros development. To examine the relationship between cloaca malformation and pronephric cysts, we utilized a transgenic zebrafish line expressing *noggin3* under the control of a

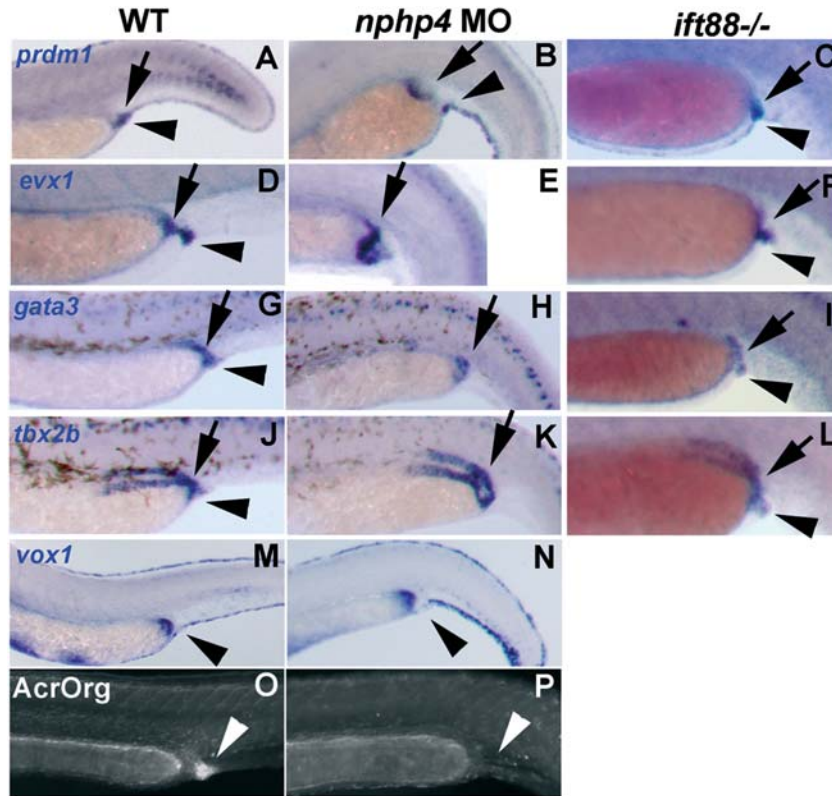


**Figure 4.** Pronephric and ectodermal components of the cloaca are correctly specified in *nphp4*-depleted embryos. (A–L) *In situ* hybridization of 2-day-old wild-type (WT), *nphp4* MO-injected and *ovl* (*ift88*<sup>-/-</sup>) zebrafish embryos stained with cloaca and epidermis (*prdm1* A–C, *evx1* D–F and *vox1* M, N) or pronephric duct (*gata3* G–I, *tbx2b* J–L) markers. In all images, an arrow marks the end of the distal pronephric duct, and an arrowhead the cloaca. The expression patterns of the markers indicate that the components of the cloaca are correctly specified, but fail to converge and to form a functional cloaca opening. (O and P) Vital stain with acridin orange dye, detecting the extent of cell death at the cloaca region 24 h post-fertilization. WT embryos were strongly labeled, revealing extensive cell death at the duct opening (arrowhead in O). Only moderate staining was detected in *nphp4* MO-injected embryos (arrowhead in P).

heat shock promoter (26). Transgenic embryos subjected to heat shock at the tail-bud stage developed pronephric cysts as well as cloaca vesicles similar to *nphp4*-depleted embryos (Supplementary Material, Fig. S1).

Bmp signaling defects prevent the programmed cell death of ectodermal cells forming the cloaca opening (17). Examination of cell death at 24 hpf using the vital dye acridine orange (AcrOrg) showed a dramatic reduction of cell death at the cloaca of *nphp4* MO-injected embryos (Fig. 4P and O). Thus, despite intact Bmp-dependent specification of the ventro-ectodermal cells, these cells fail to undergo programmed cell death, suggesting that an inductive signal from the distal pronephric duct is required to induce apoptosis of ectodermal cells, leading to cloaca opening formation.

#### *nphp4* influences cloaca formation by affecting duct cells migration

To investigate the role of zebrafish *nphp4* at the cellular level, we performed time-lapse confocal imaging of *nphp4* MO-injected and non-injected *cldb:lyn-gfp* transgenic embryos during the stages of cloaca formation (18–36 hpf). Pronephric duct cells, labeled with membrane-bound GFP, actively migrated between the yolk sac extension and the blood island to reach the epidermal cells of the proctodeum

in WT embryos (Fig. 5A–C, Supplementary Material, Movie S1). Subsequently, the cells of the pronephric duct tip migrated over the ectodermal cells in a posterior-to-anterior direction, whereby both cell types formed protrusions towards each other until the pronephric duct cells reached the position where cloaca formation occurred. Following the re-organization of the epithelial structure between epidermis and pronephric duct, some of the epidermal cells underwent apoptosis to shape the opening of the cloaca (Supplementary Material, Movie S1). Finally, the cloaca channel, formed by polarized epithelial cells of mesodermal and ectodermal origins, opened to the environment at around 30 hpf (Fig. 5G). In *nphp4* morphants, the tip cells of the distal pronephric duct failed to join the ectodermal cells committed to undergo apoptosis and to form the cloaca opening (Fig. 5D–F, G). As a consequence, the distal part of pronephric duct did not appear as a straight channel, but became distorted and formed a blunt-ended tube in *nphp4*-deficient embryos (Fig. 5D–F, G and Supplementary Material, Movie S2). Tracking of individual cells during the time of cloaca morphogenesis in WT embryos revealed that the pronephric duct cells were moving in a ventro-anterior direction, while the ectodermal cells followed a posterior direction (Fig. 5H, Supplementary Material, Movie S1). In *nphp4* MO-injected embryos, the ectodermal cells continued to move posteriorly; however, the

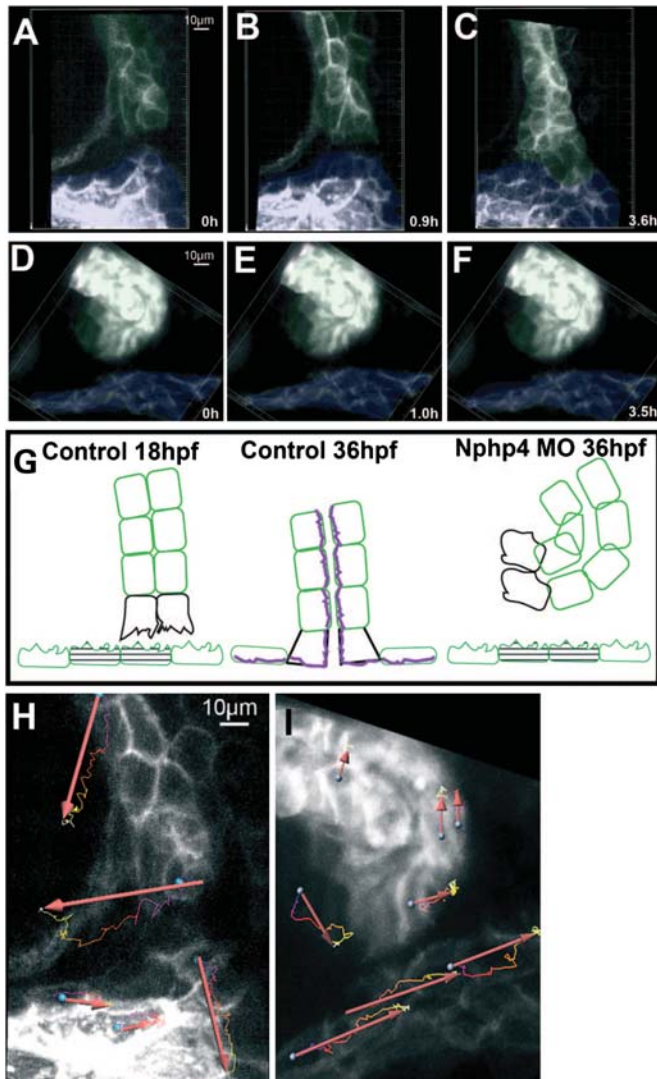


**Figure 5.** *nphp4* is required for directed cell migration of the pronephric duct cells towards the cloaca. (A–F) Images from time-lapse movies of *cld:lyn-gfp* transgenic embryos, highlighting the process of cloaca formation 18 and 36 h post-fertilization (hpf). (A–C) Pronephric duct cells of wild-type (WT) embryo migrate in a ventro-anterior direction and fuse with the ectodermal cells at the future cloaca site (Supplementary Material, Movie S1). In contrast, the distal part of the pronephric duct of morphant embryos did not exhibit directional migration (D–F) (Supplementary Material, Movie S2). (G) Schematic representation of the cloaca formation. In WT embryos, the leading tip cells of the pronephric duct are actively migrating to join cloaca-fated ectodermal cells (striped cells), which eventually undergo programmed cell death and form a tube of polarized epithelial cells that opens to the environment. The *nphp4* morphants fail to migrate towards the cloaca region and fail to induce apoptosis in the cloaca cells, resulting in a blunt end tube. (H and I) Results of individual cell-tracking experiments of WT and *nphp4* morphant embryos. The tracking was performed with Imaris software, using Supplementary Material, Movies S1 and S2. Grade-colored line represents the tracking path of the cells labeled with a blue sphere. The orange arrows represent the net direction and movement of each tracked cell. In WT embryos, pronephric duct cells are moving in an anterior–ventral direction, while the ectodermal cells move towards posterior (H). In MO-injected embryos, the ectodermal cells retain their direction, but the pronephric duct cells exhibit minimal and rather chaotic movements (I).

pronephric duct cells of *nphp4*-deficient embryos failed to display the coordinated directional movement that connects the pronephric duct tip cells with the ectodermal cells (Fig. 5I, Supplementary Material, Movie S2). Interestingly, although the leading pronephric duct cells in WT embryos exhibited typical features of migrating cells, e.g. formation of lamellipodia in the direction of migration (Supplementary Material, Movie S1), morphant cells remained stationary and failed to form cell protrusions (Supplementary Material, Movie S1). Thus, *nphp4* orchestrates the fusion of the pronephric duct with the ectoderm by supporting the directional migration of pronephric duct cells.

#### *nphp1* synergistically enhances *nphp4* cilia-related phenotypes, but not cloaca defects

Several studies have demonstrated the physical interaction between the *NPHP1* and *NPHP4* gene products (10,27), and both *NPHP1* and *NPHP4* gene products localize to the primary cilium (12). To investigate whether these two proteins synergize in zebrafish during pronephros development and cloaca formation, we designed an ATG MO, which targets zebrafish *nphp1*. At 0.4 mm, the *nphp1* MO-injected embryos developed small pronephric cysts and mild duct dilations (Supplementary Material, Fig. S3). Higher MO concentrations increased the number of malformed embryos and caused mild dorsalization with absent ventral medial fin structures. Malformed embryos also displayed cloaca obstruction, although at a low percentage (Supplementary Material, Fig. S3). Cilia length, however, remained unaltered even in embryos injected with high doses of *nphp1* MO (Supplementary Material, Fig. S3). Embryos injected with low amounts of either *nphp1* or *nphp4* MO (0.2 mM) showed mild body curvature abnormalities, but formed neither cysts nor a vesicle within the cloaca region (Fig. 6A and B). Co-injection of both MO at 0.2 mM caused a dramatic increase of the abnormal body curvature, heart edema and approximately half of the double-injected embryos formed pronephric cysts (Fig. 6C–E). Immunofluorescent analysis of the double-injected morphants with pronephric cysts revealed duct dilations and misoriented cilia (Fig. 6G–I) as well as randomized left–right asymmetry (Fig. 6F), implying defective KV function. However, cloaca vesicles were not detected in any of the double morphants. These observations suggest that *nphp1* does not synergize with *nphp4* during cloaca formation.

#### *nphp4* genetically interacts with *pard6* during cloaca formation

Since nephrocystin-4 also interacts with Par6 (10), we tested whether Par6 participates in cloaca formation. The zebrafish *pard6-gammaB* matches the murine *Pard6gamma* (28). To examine the role of *pard6-gammaB* during cloaca formation, we designed an antisense MO targeting the splice donor site of exon 2 of *pard6-gammaB* (*pard6* MO). MO-induced aberrant splicing was verified by RT–PCR (Fig. 7G); the

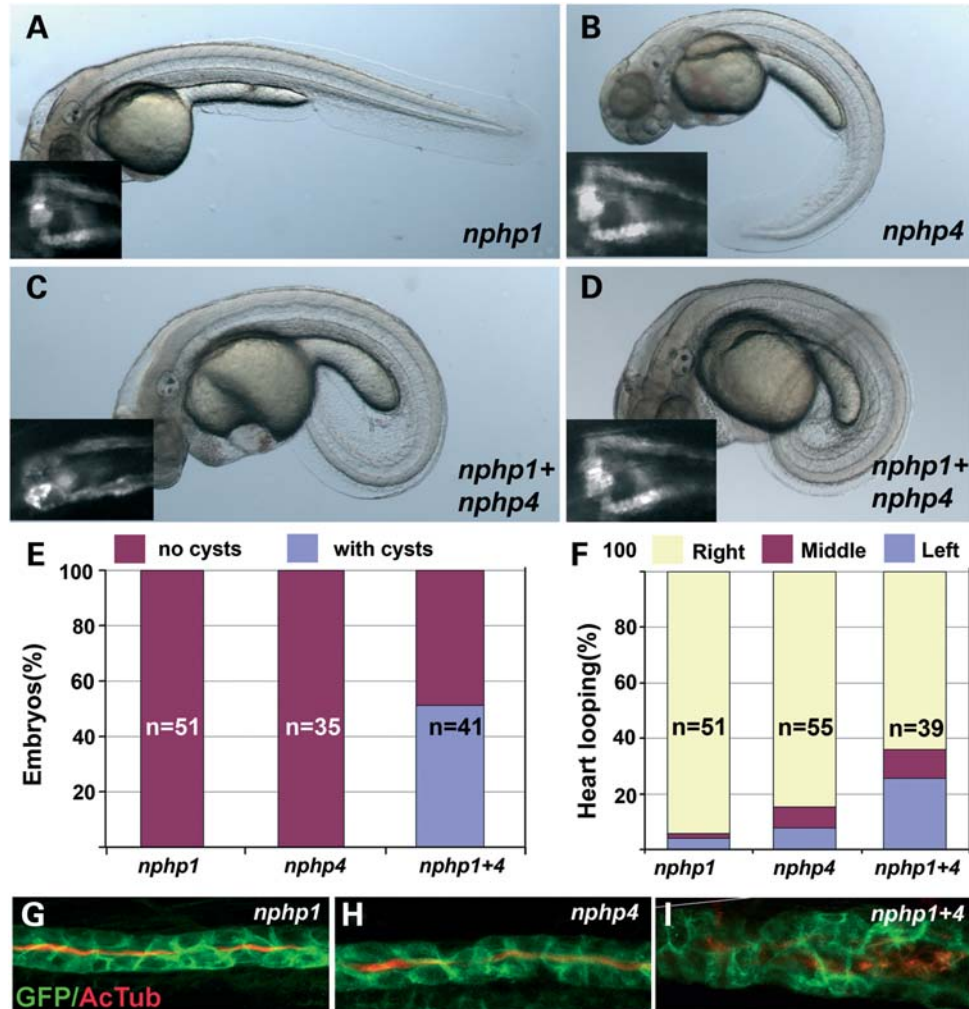


**Figure 6.** Depletion of *nphp1* does not augment cloaca malformation in *nphp4*-deficient zebrafish embryos. (A–D) Images of the *wt1b:gfp* transgenic zebrafish embryos at 2 days post-fertilization injected with 0.2 mM solution of *nphp1* (A), *nphp4* (B) or a combination of both morpholinos (C, D). The insets in every picture show a fluorescent image of the glomerulus region of the same embryo. The combined injection increased the level of body curvature and promoted cyst formation in double morphants to about 50% (C and E), but did not cause cloaca obstruction. The number of embryos with abnormal body symmetry, detected by a heart-looping defect, was also increased (F). (G–I) Confocal images of the pronephric duct of single and double MO-injected *cldb:lyn-gfp* transgenic embryos stained for GFP and acetylated tubulin. Double morphants show an increased duct diameter and disoriented cilia. These experiments suggest that cilia-dependent functions were more severely impaired in double than in single morphants.

sequence analysis revealed a deletion within the second exon of *pard6-gammaB*, leading to a frame shift and a premature STOP codon (data not shown). Depletion of *pard6* in zebrafish embryos caused mild-to-strong body curvature abnormalities and notochord undulations in a concentration-dependent manner (Fig. 7A and B and data not shown). Pericardial edema occurred in all phenotypic classes, while heart beat and blood circulation were not impaired (data not shown). The *pard6*-deficient zebrafish embryos also developed pronephric cysts, although at a low frequency ( $\leq 10\%$ ) (Fig. 7A). However, expansion of the pronephric duct lumen was observed by regular light microscopy as well as in histological sections (Fig. 7C–F). Although the cilia in the ducts of morphant embryos had a normal length, they appeared disoriented (data not shown). Injections of either 0.2 mM *nphp4* or 0.4 mM *pard6* MO in combination with a control MO to adjust the total amount of injected MO to 0.6 mM had only

moderate effects on cloaca development (Fig. 8A–D). In contrast, combined injections of 0.2 mM *nphp4* and 0.4 mM *pard6* MO caused a striking increase in the number of the embryos with obstructed cloaca (Fig. 8C and D). Time-lapse imaging of the migratory behavior of the distal pronephros showed that the cloaca forming pronephric duct cells of the double morphants failed to form protrusions directed towards the ectoderm, but only generated small blebs that quickly retracted (Fig. 8G, Supplementary Material, Movie S3). As a result, the pronephric duct failed to connect to the cloaca (Fig. 8E and F). Co-expression of human *NPHP4* mRNA ameliorated cloaca malformation caused by the *nphp4/par6* knockdown. While 33.9% of the *nphp4-pard6* double morphants ( $n = 142$ ) developed malformed cloaca, this defect was reduced to 5.9% ( $n = 125$ ) after co-injection of human *NPHP4* mRNA. These results indicate that *nphp4* acts together with components of the Par complex to orchestrate cloaca morphogenesis.

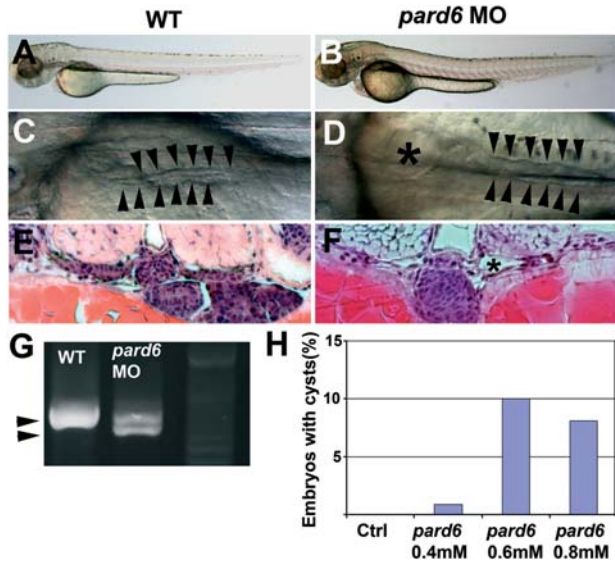


**Figure 7.** Knock down of *pard6* causes pronephric cyst formation and duct dilations. (A–D) Bright field images of 2-day-old wild-type (WT) and *pard6* MO-injected zebrafish embryos. Morphants developed mild body curvature or notochord undulations (A, B and data not shown), pronephric cysts (asterisk in D, quantified in H) and dilated tubules (arrowheads in C, D). (E and F) Cysts are clearly visible in eosin–hematoxylin histological staining of sections from WT and MO-injected embryos (asterisk in F). (G) The *pard6* MO efficiently prevents the production of functional *pard6* mRNA by blocking the splice donor site of exon 2, giving rise to an alternative splice variant with a premature stop codon.

## DISCUSSION

Knockdown of zebrafish *nphp4* leads to developmental defects commonly attributed to ciliary dysfunction, including an abnormal body curvature, *situs inversus* and formation of pronephric cysts. The reduction of ciliary length in the KV and pronephric duct of *nphp4* MO-injected embryos are consistent with the hypothesis that ciliary defects cause these morphological changes. Nephrocystin-4 localizes to the basal body of the primary cilium, and is required for normal ciliogenesis in MDCK cells. Nephrocystin-4 also interacts with components of the focal adhesion and polarity complex; however, the functional implication of these various interactions is currently poorly understood (10,12).

We now report that *nphp4*-depletion in zebrafish embryos is associated with defects in cloaca formation. We attribute this abnormality to a migratory defect of the most distal pronephric duct cells. In wild-type embryos, these cells migrate towards the prospective cloaca position and fuse with the ectodermal cells to form the cloaca opening. Our time-lapse movies revealed that the leading pronephric duct cells in *nphp4*-deficient zebrafish embryos fail to form cell protrusions and do not exhibit directional migration towards the ectodermal cells of the prospective cloaca opening.

Nephrocystin-4 forms a complex with the tight junction proteins PALS1/PATJ and Par6 proteins (10). Par6 also participates in TGF- $\beta$  signaling, a key regulator of renal fibrosis (29). Since TGF- $\beta$ -dependent phosphorylation of Par6 facilitates tight junction dissolution and epithelial-to-mesenchymal transition in mammary gland epithelial cells (30), it is

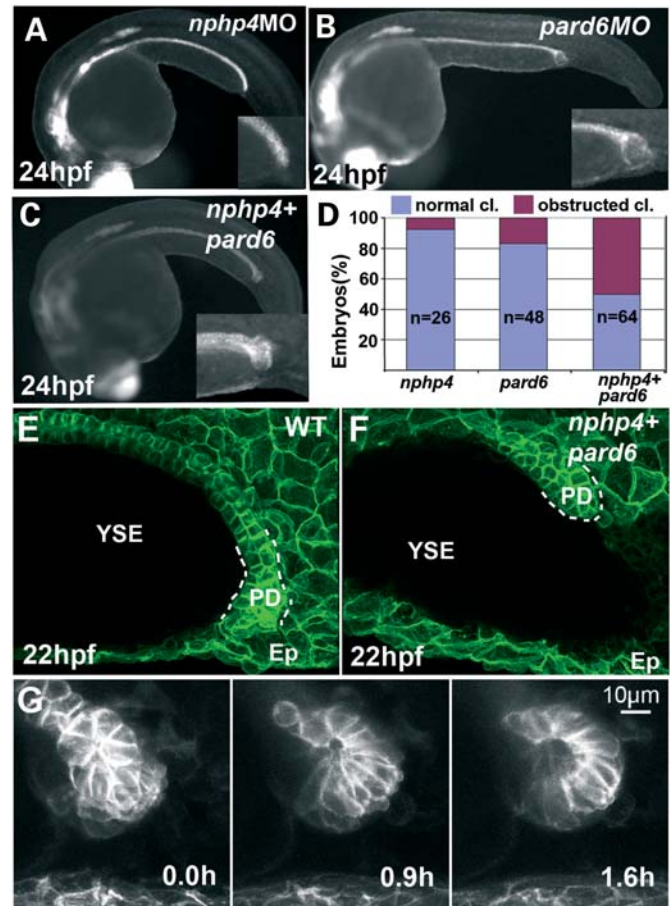


**Figure 8.** *nphp4* and *pard6* act together to promote cloaca formation in zebrafish. (A–C) Fluorescent images of embryos injected with low doses of, respectively, *nphp4* (0.2 mM) (A), *pard6* (0.4 mM) (B) and *pard6* + *nphp4* (C) morpholino (MO) at 24 h post-fertilization (hpf). The region of the cloaca is magnified in the inserts of every image. (D) Quantification of the number of cloaca obstructed embryos. There was a prominent increase in the number of affected embryos in the double morphants in comparison to the single MO injections. (E and F) Projections of confocal Z-stack images, showing the region of the cloaca of WT and *nphp4* + *pard6* MO-injected embryos at 22 hpf. Although the pronephric duct of the WT embryos has already reached the ventral fin epidermis, the duct of the double morphants remains dorsally from the yolk sac extension. (G) Images from a time-lapse movie (Supplementary Material, Movie S3) of the cloaca region of 20 hpf embryo, co-injected with *nphp4* and *pard6* MOs. The cells of the duct exhibit no directional migration, and form only small blebbing protrusions. All experiments in this figure were performed using *cldb:lyn-gfp* transgenic embryos. Ep, epidermis; PD, pronephric duct; YSE, yolk sac extension.

conceivable that nephrocystin-4 mediates the migration towards ectodermal cells through interaction with Par6. Cloaca obstruction is also observed in zebrafish embryos with defective Bmp signaling in the ventral mesoderm/proctodeum designated to form the cloaca (17,18,31). Similar to *nphp4* morphants, Bmp-defective embryos exhibit abnormal programmed cell death required for cloaca opening. However, in contrast to Bmp mutants (17,18), *prdm1* and *vox1* staining demonstrate that the ectoderm of the prospective cloaca is properly specified in *nphp4* morphants. Thus, *nphp4* appears to instruct the distal pronephric duct cells to migrate towards the ectodermal cells that subsequently undergo

apoptosis to form the cloaca opening. Our findings suggest that the programmed cell death of ectodermal cells required for cloaca formation is a non-cell autonomous, *nphp4*-dependent event, initiated by distal pronephric duct cells.

Previous studies have demonstrated the physical interaction between nephrocystin-1 and -4 (27). Our studies confirm the genetic interaction between *nphp1* and *nphp4* during zebrafish pronephros development and specification of a normal body axis; simultaneous depletion of the two proteins leads to an increase of cilia-related phenotypes, including pronephric cyst formation and laterality defects. However, *nphp1* depletion does not promote cloaca obstruction, suggesting that nephrocystin-4 acts independently of nephrocystin-1 to control the migration and fusion of distal pronephric duct cells. Our data, demonstrating that nephrocystins can autonomously engage in cellular functions may explain differences in disease manifestations observed in patients with nephropthisis.

## MATERIALS AND METHODS

### Zebrafish lines

Zebrafish of wild-type AB/TL and transgenic strains were maintained and raised as described (32). The following transgenic and mutant zebrafish strains were used: *wt1b:gfp* (19), *Cldn2b:lyn-gfp* (20), *Oval*, HSP:*noggin3* (26). Staging was performed according to Kimmel (33).

### Zebrafish embryo manipulations

Fertilized eggs were microinjected with 4 nl of injection solution at the one-to-two-cell stage with morpholino (MO; Gene Tools LLC, Philomath, OR, USA) diluted in 200 mM KCl, 0.1% Phenol Red and 10 mM HEPES. For ISHs and antibody staining, embryos were anesthetized and fixed at the desired stage in 4% PFA overnight, transferred in methanol and stored at  $-20^{\circ}\text{C}$  until stained. Two separate MOs targeting zebrafish *nphp4* were designed (Genetools), a translation-blocking MO with the sequence GCGCTTCTCCACTCAGACATCAGAG (*nphp4ATG*) and an MO targeted against the splice donor site of exon1 with the sequence ATTTATTCCCCATCCACCTGTGTCA (*nphp4 Ex1*). The MO against *nphp1*, targeted to the ATG region, had the sequence CCCTCTTCTCTTTGGAGGCATGTTG (*nphp1 ATG*). *Pard6* MO targeting splice donor site of exon 2, GAAGCGAGTGAGCTCGTACCTTGTC (*pard6 Ex2*). All MOs were co-injected with p53 MO to reduce the toxicity of these reagents (34). Phenotype rescue experiments were attempted using *in vitro* transcribed full-length human and MO-resistant zebrafish *nphp4* mRNA, which were co-injected with *nphp4ATG* MO at concentrations 100, 200 and 500 ng/ $\mu\text{l}$ .

### Imaging

Embryos were analyzed at the stage of interest under a Leica MZ16 stereo microscope (Leica, Solms, Germany). DIC and non-confocal fluorescent images were taken with a SPOT Insight Fire Wire System (Diagnostic Instruments, Sterling Heights, MI, USA). Confocal images and confocal time-lapse

movies were taken with Zeiss LSM510 microscope and processed with LSM (Zeiss) and Imaris (Bitplain) software.

### Immunohistochemistry and ISH

ISH was performed as described previously (35). Antisense probes for *nphp4*, *prdm1*, *tbx2b* and *gata3* were amplified from zebrafish embryonic cDNA, cloned in TOPO (Invitrogen) and linearized with corresponding restriction enzymes. Dig-labeled antisense RNA was synthesized using Roche Dig labeling kit (Roche). Primary antibodies rabbit polyclonal anti-GFP (Biozol), rabbit anti-PKC zeta (Santa Cruz) and mouse anti-acetylated tubulin (Sigma) were used in a 1:500 dilution. Secondary anti-mouse and anti-rabbit antibodies labeled with Alexa488, Alexa546 or Cy3 antibodies were obtained from Jackson Immuno Research Laboratories. For imaging the cilia of the KV, 6-somite-stage embryos were fixed in Dent's fixative and stained for acetylated tubulin. The KV region was dissected, embedded in fluoromount and imaged using confocal microscopy.

### Paraffin sections and eosin/hematoxylin staining

For histological studies, embryos were anesthetized and fixed O/N in 4% PFA. Further, embryos were dehydrated in ethanol series, cleared in toluol and embedded in paraffin wax. Six-micrometer-thick sections were cut using a microtome (Leica), stained for Hematoxylin and Eosin and imaged with an Axioplan2 microscope and AxioVision software (Zeiss, Germany).

### Time-lapse imaging of cell migration

For time-lapse movies, we used un-injected and MO-injected *Cldb:Lyn-gfp* zebrafish embryos (20). The embryos were embedded in 1.5% low-melting agarose, and imaged over time at 40x, using a Zeiss LSM510 confocal microscope. Z-stacks were acquired every 3 min and processed with Imaris software.

### Acridine orange staining

To assay the levels of cell death in the cloaca region, 30 hpf embryos were dechorionated and incubated in 2  $\mu\text{g/ml}$  acridine orange (Sigma) solution in E3 medium for 30 min. The embryos were then washed repeatedly, embedded in low-melting agarose and imaged using a Leica MZ16 stereo microscope.

## SUPPLEMENTARY MATERIAL

Supplementary Material is available at *HMG* online.

*Conflict of Interest statement.* None declared.

## FUNDING

This work was supported by the German Research Council (DFG) (to A.K.-Z., G.W.) and by the European Community's

Seventh Framework Program (grant agreement number 241955, SYSCILIA) (to G.W.).

## REFERENCES

- Hildebrandt, F., Attanasio, M. and Otto, E. (2009) Nephronophthisis: disease mechanisms of a ciliopathy. *J. Am. Soc. Nephrol.*, **20**, 23–35.
- Hildebrandt, F. and Zhou, W. (2007) Nephronophthisis-associated ciliopathies. *J. Am. Soc. Nephrol.*, **18**, 1855–1871.
- Hurd, T.W. and Hildebrandt, F. (2011) Mechanisms of nephronophthisis and related ciliopathies. *Nephron*, **118**, e9–e14.
- Wolf, M.T. and Hildebrandt, F. (2011) Nephronophthisis. *Pediatr. Nephrol.*, **26**, 181–194.
- Liu, S., Lu, W., Obara, T., Kuida, S., Lehoczy, J., Dewar, K., Drummond, I.A. and Beier, D.R. (2002) A defect in a novel Nek-family kinase causes cystic kidney disease in the mouse and in zebrafish. *Development*, **129**, 5839–5846.
- Otto, E.A., Helou, J., Allen, S.J., O'Toole, J.F., Wise, E.L., Ashraf, S., Attanasio, M., Zhou, W., Wolf, M.T. and Hildebrandt, F. (2008) Mutation analysis in nephronophthisis using a combined approach of homozygosity mapping, CEL I endonuclease cleavage, and direct sequencing. *Hum. Mut.*, **29**, 418–426.
- Sayer, J.A., Otto, E.A., O'Toole, J.F., Nurnberg, G., Kennedy, M.A., Becker, C., Hennies, H.C., Helou, J., Attanasio, M., Fausett, B.V. *et al.* (2006) The centrosomal protein nephrocystin-6 is mutated in Joubert syndrome and activates transcription factor ATF4. *Nat. Genet.*, **38**, 674–681.
- Schafer, T., Putz, M., Lienkamp, S., Ganner, A., Bergbreiter, A., Ramachandran, H., Gieloff, V., Gerner, M., Mattonet, C., Czarniecki, P.G. *et al.* (2008) Genetic and physical interaction between the NPHP5 and NPHP6 gene products. *Hum. Mol. Genet.*, **17**, 3655–3662.
- Goetz, S.C. and Anderson, K.V. (2010) The primary cilium: a signalling centre during vertebrate development. *Nat. Rev.*, **11**, 331–344.
- Delous, M., Hellman, N.E., Gaude, H.M., Silbermann, F., Le Bivic, A., Salomon, R., Antignac, C. and Saunier, S. (2009) Nephrocystin-1 and nephrocystin-4 are required for epithelial morphogenesis and associate with PALS1/PATJ and Par6. *Hum. Mol. Genet.*, **18**, 4711–4723.
- Donaldson, J.C., Dempsey, P.J., Reddy, S., Bouton, A.H., Coffey, R.J. and Hanks, S.K. (2000) Crk-associated substrate p130(Cas) interacts with nephrocystin and both proteins localize to cell-cell contacts of polarized epithelial cells. *Exp. Cell Res.*, **256**, 168–178.
- Mollet, G., Silbermann, F., Delous, M., Salomon, R., Antignac, C. and Saunier, S. (2005) Characterization of the nephrocystin/nephrocystin-4 complex and subcellular localization of nephrocystin-4 to primary cilia and centrosomes. *Hum. Mol. Genet.*, **14**, 645–656.
- Roepman, R., Letteboer, S.J., Arts, H.H., van Beersum, S.E., Lu, X., Krieger, E., Ferreira, P.A. and Cremers, F.P. (2005) Interaction of nephrocystin-4 and RPGRIP1 is disrupted by nephronophthisis or Leber congenital amaurosis-associated mutations. *Proc. Natl Acad. Sci. USA*, **102**, 18520–18525.
- Drummond, I.A. (2005) Kidney development and disease in the zebrafish. *J. Am. Soc. Nephrol.*, **16**, 299–304.
- Kramer-Zucker, A.G., Wiessner, S., Jensen, A.M. and Drummond, I.A. (2005) Organization of the pronephric filtration apparatus in zebrafish requires Nephhrin, Podocin and the FERM domain protein Mosaic eyes. *Dev. Biol.*, **285**, 316–329.
- Sullivan-Brown, J., Schottenfeld, J., Okabe, N., Hostetter, C.L., Serluca, F.C., Thiberge, S.Y. and Burdine, R.D. (2008) Zebrafish mutations affecting cilia motility share similar cystic phenotypes and suggest a mechanism of cyst formation that differs from pkd2 morphants. *Dev. Biol.*, **314**, 261–275.
- Pyati, U.J., Cooper, M.S., Davidson, A.J., Nechiporuk, A. and Kimelman, D. (2006) Sustained Bmp signaling is essential for cloaca development in zebrafish. *Development*, **133**, 2275–2284.
- Stickney, H.L., Imai, Y., Draper, B., Moens, C. and Talbot, W.S. (2007) Zebrafish bmp4 functions during late gastrulation to specify ventroposterior cell fates. *Dev. Biol.*, **310**, 71–84.
- Perner, B., Englert, C. and Bollig, F. (2007) The Wilms tumor genes wt1a and wt1b control different steps during formation of the zebrafish pronephros. *Dev. Biol.*, **309**, 87–96.
- Haas, P. and Gilmour, D. (2006) Chemokine signaling mediates self-organizing tissue migration in the zebrafish lateral line. *Dev. Cell*, **10**, 673–680.
- Serluca, F.C., Xu, B., Okabe, N., Baker, K., Lin, S.Y., Sullivan-Brown, J., Konieczkowski, D.J., Jaffe, K.M., Bradner, J.M., Fishman, M.C. *et al.* (2009) Mutations in zebrafish leucine-rich repeat-containing six-like affect cilia motility and result in pronephric cysts, but have variable effects on left-right patterning. *Development*, **136**, 1621–1631.
- Essner, J.J., Amack, J.D., Nyholm, M.K., Harris, E.B. and Yost, H.J. (2005) Kupffer's vesicle is a ciliated organ of asymmetry in the zebrafish embryo that initiates left-right development of the brain, heart and gut. *Development*, **132**, 1247–1260.
- Kramer-Zucker, A.G., Olale, F., Haycraft, C.J., Yoder, B.K., Schier, A.F. and Drummond, I.A. (2005) Cilia-driven fluid flow in the zebrafish pronephros, brain and Kupffer's vesicle is required for normal organogenesis. *Development*, **132**, 1907–1921.
- Wilm, T.P. and Solnica-Krezel, L. (2005) Essential roles of a zebrafish prdm1/blimp1 homolog in embryo patterning and organogenesis. *Development*, **132**, 393–404.
- Thaeron, C., Avaron, F., Casane, D., Borday, V., Thisse, B., Thisse, C., Boulekbache, H. and Laurenti, P. (2000) Zebrafish evx1 is dynamically expressed during embryogenesis in subsets of interneurons, posterior gut and urogenital system. *Mech. Dev.*, **99**, 167–172.
- Chocron, S., Verhoeven, M.C., Rentzsch, F., Hammerschmidt, M. and Bakkens, J. (2007) Zebrafish Bmp4 regulates left-right asymmetry at two distinct developmental time points. *Dev. Biol.*, **305**, 577–588.
- Mollet, G., Salomon, R., Gribouval, O., Silbermann, F., Bacq, D., Landthaler, G., Milford, D., Nayir, A., Rizzoni, G., Antignac, C. *et al.* (2002) The gene mutated in juvenile nephronophthisis type 4 encodes a novel protein that interacts with nephrocystin. *Nat. Genet.*, **32**, 300–305.
- Munson, C., Huisken, J., Bit-Avragim, N., Kuo, T., Dong, P.D., Ober, E.A., Verkade, H., Abdelilah-Seyfried, S. and Stainier, D.Y. (2008) Regulation of neurocoel morphogenesis by Pard6 gamma b. *Dev. Biol.*, **324**, 41–54.
- Bottinger, E.P. (2007) TGF-beta in renal injury and disease. *Sem. Nephrol.*, **27**, 309–320.
- Ozdamar, B., Bose, R., Barrios-Rodiles, M., Wang, H.R., Zhang, Y. and Wrana, J.L. (2005) Regulation of the polarity protein Par6 by TGFbeta receptors controls epithelial cell plasticity. *Science*, **307**, 1603–1609.
- Hammerschmidt, M., Serbedzija, G.N. and McMahon, A.P. (1996) Genetic analysis of dorsoventral pattern formation in the zebrafish: requirement of a BMP-like ventralizing activity and its dorsal repressor. *Gene Dev.*, **10**, 2452–2461.
- Westerfield, M. (1995) *The Zebrafish Book: A Guide for the Laboratory Use of Zebrafish (Danio rerio)*. University of Oregon Press, Eugene.
- Kimmel, C.B. (1989) Genetics and early development of zebrafish. *Trend. Genet.*, **5**, 283–288.
- Robu, M.E., Larson, J.D., Nasevicius, A., Beiraghi, S., Brenner, C., Farber, S.A. and Ekker, S.C. (2007) p53 activation by knockdown technologies. *PLoS Genet.*, **3**, e78.
- Fu, X., Wang, Y., Schetle, N., Gao, H., Putz, M., von Gersdorff, G., Walz, G. and Kramer-Zucker, A.G. (2008) The subcellular localization of TRPP2 modulates its function. *J. Am. Soc. Nephrol.*, **19**, 1342–1351.